

# Beyond $Ti_3C_2T_x$ : MXenes for Electromagnetic Interference Shielding

*Meikang Han<sup>1</sup>, Christopher Eugene Shuck<sup>1</sup>, Roman Rakhmanov<sup>1, 2</sup>, David Parchment<sup>1</sup>, Babak Anasori<sup>1, 3</sup>, Chong Min Koo<sup>4</sup>, Gary Friedman<sup>2</sup> and Yury Gogotsi<sup>1\*</sup>*

<sup>1</sup>A. J. Drexel Nanomaterials Institute and Department of Materials Science and Engineering,  
Drexel University, Philadelphia, PA 19104, USA

<sup>2</sup>Department of Electrical and Computer Engineering, Drexel University, Philadelphia, PA  
19104, USA

<sup>3</sup>Department of Mechanical and Energy Engineering, Integrated Nanosystems Development  
Institute, Purdue School of Engineering and Technology, Indiana University–Purdue University  
Indianapolis, Indianapolis, IN 46202, USA

<sup>4</sup>Materials Architecturing Research Centre, Korea Institute of Science and Technology (KIST),  
Seoul 02792, Korea

\* Corresponding author: Prof. Yury Gogotsi (Y. G.), E-mail: [gogotsi@drexel.edu](mailto:gogotsi@drexel.edu).

---

This is the author's manuscript of the article published in final edited form as:

Han, M., Shuck, C. E., Rakhmanov, R., Parchment, D., Anasori, B., Koo, C. M., ... & Gogotsi, Y. Beyond  $Ti_3C_2T_x$ : MXenes for Electromagnetic Interference Shielding. *ACS Nano*. <https://doi.org/10.1021/acsnano.0c01312>

1  
2  
3 ABSTRACT  
4  
5  
6

7 New ultrathin and multifunctional electromagnetic interference (EMI) shielding materials  
8 are required for protecting electronics against electromagnetic pollution in the fifth-generation  
9 networks and Internet of Things era. Micrometer-thin  $\text{Ti}_3\text{C}_2\text{T}_x$  MXene films have shown the best  
10 EMI shielding performance among synthetic materials so far. Yet, the effects of elemental  
11 composition, layer structure, and transition metal arrangement on EMI shielding properties of  
12 MXenes have not been explored, despite the fact that more than 30 different MXenes have been  
13 reported and many more are possible. Here, we report on a systematic study of EMI shielding  
14 properties of 16 different MXenes, which cover single-metal MXenes, ordered double-metal  
15 carbide MXenes, and random solid solution MXenes of M and X elements. This is the largest set  
16 of MXene compositions ever reported in a comparative study. Films with thicknesses ranging  
17 from nanometers to micrometers were produced by spin-casting, spray-coating, and vacuum-  
18 assisted filtration. All MXenes achieved effective EMI shielding (>20 dB) in micrometer-thick  
19 films. The EMI shielding effectiveness of sprayed  $\text{Ti}_3\text{C}_2\text{T}_x$  film with a thickness of only ~40 nm  
20 reaches 21 dB. Adjustable EMI shielding properties were achieved in solid solution MXenes  
21 with different ratios of elements. A transfer matrix model was shown to fit EMI shielding data  
22 for highly conductive MXenes, but could not describe the behavior of materials with low  
23 conductivity. This work shows that many members of the large MXene family can be used for  
24 EMI shielding, contributing to designing ultrathin, flexible, and multifunctional EMI shielding  
25 films benefitting from specific characteristics of individual MXenes.  
26  
27  
28  
29  
30  
31  
32  
33  
34  
35  
36  
37  
38  
39  
40  
41  
42  
43  
44  
45  
46  
47  
48  
49  
50

51  
52 KEYWORDS: MXene, two-dimensional, electromagnetic interference shielding, conductivity,  
53  
54 film  
55  
56  
57  
58  
59  
60

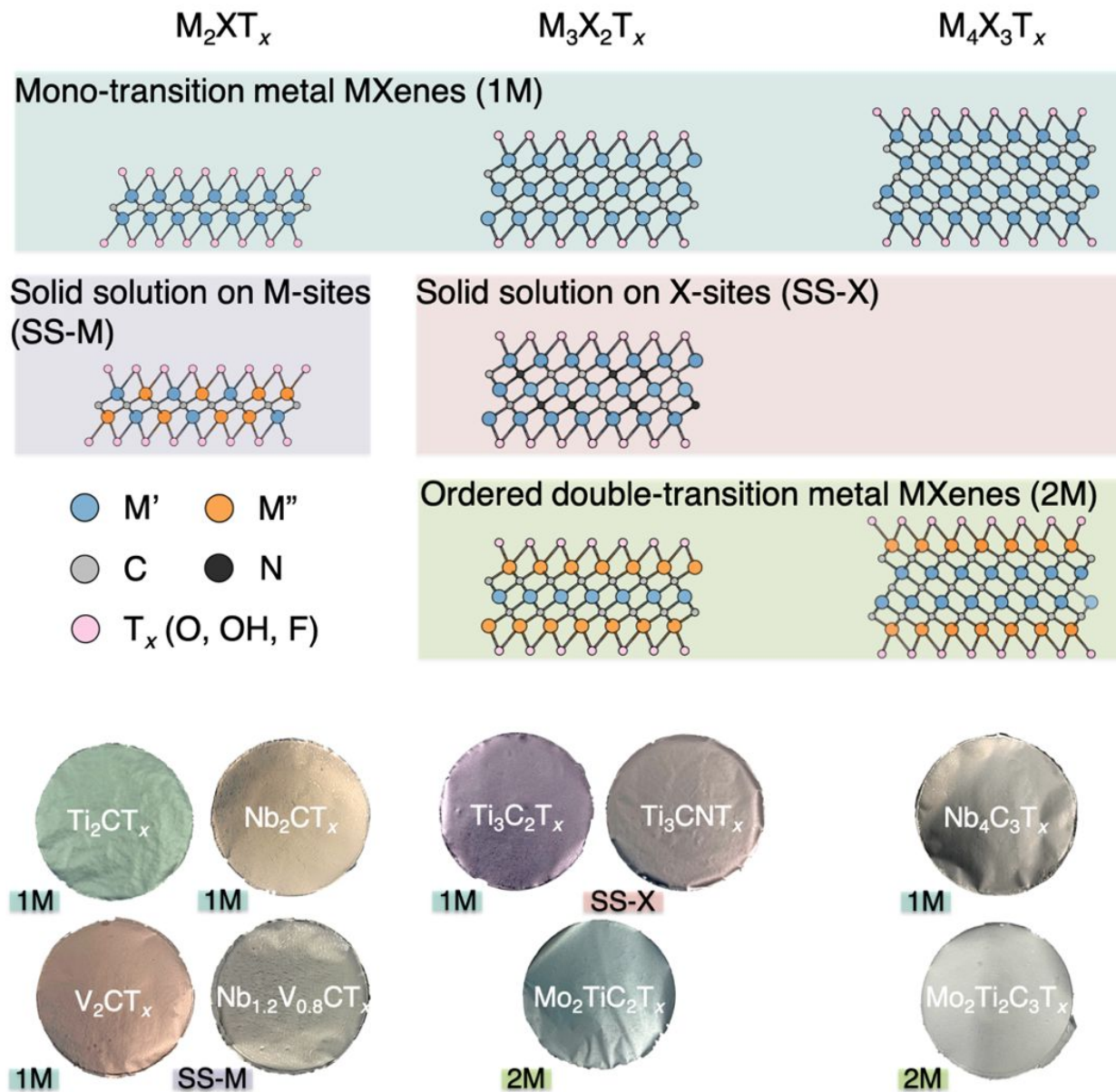
1  
2  
3 The arrival of commercial fifth generation (5G; 450 MHz—52 GHz) networks and a significant  
4 increase in the number of wireless Internet of Things (IoT) devices working across diverse  
5 frequency ranges made communication stability and security without electromagnetic  
6 interference (EMI) a critical requirement.<sup>1</sup> Specifically, for flexible wearable devices and  
7 miniaturized electronics with complex architectures, such as electronic skins, sensors, Bluetooth  
8 components, *etc.*, it has become more challenging to confront the selective jamming in different  
9 frequency ranges.<sup>2</sup>

10  
11  
12  
13  
14  
15  
16  
17  
18  
19  
20  
21 Conventional metals (Ag, Cu, Ni, and others) provide excellent barriers against  
22 electromagnetic waves, but metal foils cannot be used in tiny microelectronic devices and  
23 deposition of thin metal films onto uneven device surfaces is not an easy task.<sup>3,4</sup> In addition, EMI  
24 shielding effectiveness (SE) of metal coatings is limited by the skin depths of metals, decreasing  
25 efficiency of ultrathin metal coatings and limiting their use in wearable and portable electronic  
26 devices.<sup>5</sup> Graphene, which has low density, high strength, and excellent chemical stability, was  
27 considered until recently as the most promising alternative to replace metals for EMI shielding.<sup>6,7</sup>  
28 In 2016,  $Ti_3C_2T_x$  ( $T_x$  represents the surface termination groups) MXene films were demonstrated  
29 to have outstanding EMI shielding capability at micrometer-scale thickness, outperforming both  
30 metals and carbon materials (graphene, carbon nanotubes and carbon fibers).<sup>8</sup> Since then,  
31 tremendous efforts focused on optimizing the EMI shielding performance of  $Ti_3C_2T_x$  and  
32 manufacturing of  $Ti_3C_2T_x$  aerogels,  $Ti_3C_2T_x$ /polymer composites, and  $Ti_3C_2T_x$ /carbon hybrids.<sup>9-14</sup>  
33 MXenes are produced by a scalable selective etching in acidic solutions, that leads to -O, -OH  
34 and -F surface terminations making them solution-processable and available for various coating  
35 manufacturing techniques, including spray-coating, spin-casting, inkjet printing, dip-coating and  
36 interfacial assembly.<sup>15-18</sup> In addition, these functionalized surfaces facilitate adhesion and  
37  
38  
39  
40  
41  
42  
43  
44  
45  
46  
47  
48  
49  
50  
51  
52  
53  
54  
55  
56  
57  
58  
59  
60

1  
2  
3 bonding to substrates. All the above advantages indicate that MXene is an alternative to the  
4 conventional metals and carbon materials for EMI shielding. However, few studies have  
5 explored the EMI shielding properties of MXenes other than  $Ti_3C_2T_x$ , although more than 30  
6 kinds of MXenes with different compositions and structures have been published.<sup>19</sup>  
7  
8  
9

10  
11  
12  
13 MXenes are typically synthesized from MAX phases, which have the general formula  
14  $M_{n+1}AX_n$  ( $n=1-4$ ).<sup>20</sup> There are three common MAX phase structures,  $M_2AX$ ,  $M_3AX_2$  and  
15  $M_4AX_3$ , where M represents the early transition metal, A is an A-group element of group 13 to  
16 15 of the periodic table, and X is carbon and/or nitrogen.<sup>21,22</sup> Consequently, MXenes commonly  
17 have three structures:  $M_2XT_x$ ,  $M_3X_2T_x$  and  $M_4X_3T_x$ , as shown in **Figure 1**. Based on the different  
18 M and X elements, they can also be sorted as mono-metal MXenes, double-metal ( $M'$  and  $M''$ )  
19 MXenes, and double-X (C and N - carbonitrides) solid solution MXenes. Double-metal MXenes  
20 exist in two different forms, depending on the distribution of  $M'$  and  $M''$  metals: 1) solid solution  
21 MXenes where the M-sites are randomly occupied by two kinds of metal atoms and 2) ordered  
22 MXenes where the  $M'$  and  $M''$  elements are separated into different layers (Figure 1). To date,  
23 most MXenes show active surfaces and good dispersion in water and some organic solvents due  
24 to the acid-etching process.<sup>23</sup> Therefore, the MXene family is a promising platform for  
25 multifunctional EMI shielding coatings/devices.  
26  
27  
28  
29  
30  
31  
32  
33  
34  
35  
36  
37  
38  
39  
40  
41  
42  
43

44 Despite the fact that the EMI shielding properties of  $Ti_3C_2T_x$  have been explored  
45 extensively, little is known about the effects of layer structure, elemental composition, or metal  
46 element arrangement on EMI shielding performance. Here, we synthesized 16 different MXenes,  
47 comprising various elemental compositions and structures that include the three primary classes  
48 of MXenes, including mono-metal MXenes, ordered double-metal MXenes, and random solid  
49  
50  
51  
52  
53  
54  
55  
56  
57  
58  
59  
60



44  
45  
46  
47  
48  
49  
50  
51  
52  
53  
54  
55  
56  
57  
58  
59  
60

**Figure 1. MXenes synthesized in this work.** Atomic structures viewed from the [110] zone axis for three types of MXenes ( $M_2XT_x$ ,  $M_3X_2T_x$  and  $M_4X_3T_x$ , where T is shown as a bridging oxygen on the surface). They also can be sorted into four different kinds: mono-transition metal MXenes (1M), solid solution on M-sites (SS-M), solid solution on X-sites (SS-X (C and N)), and ordered double-transition metal MXenes (2M). Digital images of vacuum-filtrated freestanding films from different MXene colloidal solutions. ‘1M’ MXene films:  $M_2CT_x$  ( $Ti_2CT_x$ ,  $Nb_2CT_x$  and  $V_2CT_x$ ),  $Ti_3C_2T_x$ , and  $Nb_4C_3T_x$ ; SS-M MXene films:  $Ti_yNb_{2-y}CT_x$  and  $Nb_yV_{2-y}CT_x$  ( $y = 0.4, 0.8, 1.2$  and  $1.6$ ); eight solid solutions on M-sites MXenes with different ratios of metal elements were synthesized in this work, here  $Nb_{1.2}V_{0.8}CT_x$  film is as an example; ‘2M’ MXene films:  $Mo_2TiC_2T_x$  and  $Mo_2Ti_2C_3T_x$ ; ‘SS-X’ MXene film:  $Ti_3CNT_x$ . The film diameter is 47 mm.

1  
2  
3 solution MXenes (Figure 1). The EMI shielding performance of MXene films with the  
4 thicknesses from nano to microscale has been investigated. Fitting of the results for different  
5 MXenes with a transfer matrix model provides some insights into the relationships between their  
6 EMI shielding properties and frequency/thickness/electrical conductivity. The produced very  
7 large set of EMI shielding capability data for the MXene family enables the rational design of  
8 EMI shielding coatings using different MXenes.  
9  
10  
11  
12  
13  
14  
15  
16  
17  
18  
19

## 20 RESULTS AND DISCUSSION

21  
22 Sixteen different MAX phases, including mono-M ( $\text{Ti}_2\text{AlC}_2$ ,  $\text{V}_2\text{AlC}_2$ , and  $\text{Nb}_2\text{AlC}_2$ ) and  
23 solid solution  $\text{M}_2\text{AX}$  ( $\text{Ti}_y\text{Nb}_{2-y}\text{AlC}$  and  $\text{Nb}_y\text{V}_{2-y}\text{AlC}$  ( $y = 0.4, 0.8, 1.2$  and  $1.6$ )),  $\text{M}_3\text{AX}_2$   
24 ( $\text{Ti}_3\text{AlC}_2$ ,  $\text{Ti}_3\text{AlCN}$  and  $\text{Mo}_2\text{TiAlC}_2$ ), and  $\text{M}_4\text{AX}_3$  ( $\text{Nb}_4\text{AlC}_3$  and  $\text{Mo}_2\text{Ti}_2\text{AlC}_2$ ), were initially  
25 synthesized. All synthesis conditions were summarized in Table S1. X-ray diffraction (XRD)  
26 patterns of all MAX phases are shown in Figure S2. Correspondingly, 16 different MXenes were  
27 obtained by the selective removal of the Al layers from MAX phase precursors using different  
28 etching and delamination processes. Figure 1 shows the freestanding MXene films prepared *via*  
29 vacuum-assisted filtration from the colloidal MXene solutions. MXenes have widely differing  
30 optical properties, which can be visually observed in the freestanding films.<sup>17,24</sup> These films  
31 represent the primary MXene categories: A) mono-M MXenes.  $\text{Ti}_2\text{CT}_x$  (green),  $\text{Nb}_2\text{CT}_x$  (gold),  
32  $\text{V}_2\text{CT}_x$  (bronze),  $\text{Ti}_3\text{C}_2\text{T}_x$  (purple) and  $\text{Nb}_4\text{C}_3\text{T}_x$  (dark grey); B) double-X MXene.  $\text{Ti}_3\text{CNT}_x$   
33 ( $\text{Ti}_3\text{CNT}_x$  (violet black)); C) double-M MXenes.  $\text{Mo}_2\text{TiC}_2\text{T}_x$  (silver grey),  $\text{Mo}_2\text{Ti}_2\text{C}_3\text{T}_x$  (silver),  $\text{Ti}_y\text{Nb}_{2-y}\text{CT}_x$   
34 and  $\text{Nb}_y\text{V}_{2-y}\text{CT}_x$ . Of these,  $\text{Mo}_2\text{TiC}_2\text{T}_x$  and  $\text{Mo}_2\text{Ti}_2\text{C}_3\text{T}_x$  are ordered with the arrangement of Mo-  
35 Ti-Mo and Mo-Ti-Ti-Mo, respectively.<sup>25</sup>  $\text{Ti}_y\text{Nb}_{2-y}\text{CT}_x$  and  $\text{Nb}_y\text{V}_{2-y}\text{CT}_x$  are random solid  
36 solutions whose colors change based on their specific chemical compositions. All the elemental  
37  
38  
39  
40  
41  
42  
43  
44  
45  
46  
47  
48  
49  
50  
51  
52  
53  
54  
55  
56  
57  
58  
59  
60

1  
2  
3 ratios for  $Ti_yNb_{2-y}CT_x$  and  $Nb_yV_{2-y}CT_x$  are based on compositions of solid solution MAX phases,  
4  
5 assuming no transition metal loss during etching. Complete delamination of all MXenes was  
6  
7 confirmed by XRD patterns of the MXene films (Figure S3). All of them show a prominent  
8  
9 (002) diffraction peak of MXene at  $2\theta = \sim 5.3\text{-}7.3^\circ$ . For all systems where the MAX is converted  
10  
11 to MXene, the Al layer is removed, and replaced with the surface terminations, in addition to  
12  
13 water and intercalants between the layers, leading to enlarged  $d$ -spacing compared to MAX  
14  
15 phase precursors.<sup>26</sup> Hence, the observed  $d$ -spacing values are related to both the thickness of the  
16  
17 MXene flakes ( $n$ ) and the intercalants. For example, the (002) peaks  $d$ -spacing of  $Ti_2AlC$ ,  
18  
19  $Ti_3AlC_2$ , and  $Nb_4AlC_3$  is 6.7 Å ( $2\theta = 13.1^\circ$ ), 9.2 Å ( $2\theta = 9.60^\circ$ ), and 12.0 Å ( $2\theta = 7.36^\circ$ ),  
20  
21 respectively. After conversion of these MAX phases into MXenes, the (002) peak  $d$ -spacing of  
22  
23  $Ti_2CT_x$ ,  $Ti_3C_2T_x$ , and  $Nb_4C_3T_x$  increased to 12.1 Å ( $2\theta = 7.28^\circ$ ), 12.6 Å ( $2\theta = 7.00^\circ$ ), and 16.6 Å  
24  
25 ( $2\theta = 5.32^\circ$ ), respectively. The  $d$ -spacing expansion from  $M_2XT_x$ ,  $M_3X_2T_x$  to  $M_4X_3T_x$  can be due  
26  
27 to the presence of intercalants, such as TMAOH, used to delaminate MXene, and water  
28  
29 molecules.  
30  
31  
32  
33  
34  
35

36 To investigate the EMI shielding performance of different MXenes, spin-casting, spray-  
37  
38 coating, and vacuum-assisted filtration were used to fabricate MXene films of various thickness.  
39  
40 For MXene films with a thickness of  $\sim 2$  nm, we used a 130  $\mu\text{m}$ -thick glass slide with negligible  
41  
42 EMI SE as substrate (Figure S4), and deposited  $Ti_2CT_x$  and  $Ti_3C_2T_x$  films by spin-casting. Spray-  
43  
44 coating was used to fabricate  $< 150$  nm  $Ti_2CT_x$  and  $Ti_3C_2T_x$  films. Using vacuum-assisted  
45  
46 filtration of the colloidal MXene solutions,  $\sim 1\text{-}15$   $\mu\text{m}$  thick MXene films were prepared. All  
47  
48 vacuum-filtered MXene films were freestanding and flexible, which is attributed to the 2D  
49  
50 morphology of the delaminated MXene flakes (Figure 2a, b). All MXenes investigated here have  
51  
52 similar 2D morphologies with varying lateral dimensions. As an example,  $Ti_2CT_x$  flakes and  
53  
54  
55  
56  
57  
58  
59  
60

1  
2  
3 films are presented in Figure 2a-d. Both spray-coated films and filtered films show a similar  
4 aligned layered structure in cross-section (Figures 2c and 2d). It is noteworthy that the spray-  
5 coated films have better (more planar) stacking order than the filtered films owing to the layer-  
6 by-layer drying process. This was further confirmed by surface roughness analysis of spin-cast  
7 and spray-coated films using optical and SEM images (Figure S5). The density of spray-coated  
8  $\text{Ti}_3\text{C}_2\text{T}_x$  films was  $\sim 3.8 \text{ g cm}^{-3}$  while that of filtered  $\text{Ti}_3\text{C}_2\text{T}_x$  films was  $\sim 2.7 \text{ g cm}^{-3}$ . The more  
9 uniform stacked layers lead to a higher film density (better interflake contact), which results in a  
10 higher electrical conductivity.  
11  
12  
13  
14  
15  
16  
17  
18  
19  
20  
21

22 Figures 2e-g show the total EMI SE ( $\text{SE}_T$ ) values for all MXene films of similar  
23 thicknesses ( $5 \pm 0.3 \mu\text{m}$ ) in the X-band (8.2-12.4 GHz). All exhibit a quasilinear frequency-  
24 dependent behavior whereby the  $\text{SE}_T$  decreases with increasing frequency. This indicates that all  
25 studied MXenes have a similar frequency-dependent conductive behavior. When the film  
26 thickness is  $\sim 5 \mu\text{m}$ , the total EMI SE values of all MXenes, except  $\text{Nb}_2\text{CT}_x$  and  $\text{Mo}_2\text{TiC}_2\text{T}_x$ ,  
27 exceed 20 dB which means  $> 99\%$  shielding efficiency in the whole X-band (Figure 2e). It was  
28 observed that Ti-based MXenes ( $\text{Ti}_2\text{CT}_x$ ,  $\text{Ti}_3\text{CNT}_x$ , and  $\text{Ti}_3\text{C}_2\text{T}_x$ ) with  $\text{SE}_T$  values above 40 dB  
29 have better EMI shielding performance than other MXenes. In particular, the performance of  
30 solid-solution MXenes ( $\text{Ti}_y\text{Nb}_{2-y}\text{CT}_x$  and  $\text{Nb}_y\text{V}_{2-y}\text{CT}_x$ ) was compared with mono-M  $\text{M}_2\text{CT}_x$   
31 MXenes ( $\text{Ti}_2\text{CT}_x$ ,  $\text{Nb}_2\text{CT}_x$ , and  $\text{V}_2\text{CT}_x$ ), as shown in Figure 2f, g. For  $\text{Ti}_y\text{Nb}_{2-y}\text{CT}_x$ , their  $\text{SE}_T$   
32 values are between  $\text{Ti}_2\text{CT}_x$  and  $\text{Nb}_2\text{CT}_x$ , and increase with the atomic ratio of Ti. Similarly, the  
33  $\text{SE}_T$  values of  $\text{Nb}_y\text{V}_{2-y}\text{CT}_x$  increase with the amount of V. These trends indicate that the EMI  
34 shielding properties of solid-solution MXenes are tunable by controlling of the M'/M'' ratios. We  
35 further studied the reflection and absorption behavior of different MXenes. The average EMI SE  
36  
37  
38  
39  
40  
41  
42  
43  
44  
45  
46  
47  
48  
49  
50  
51  
52  
53  
54  
55  
56  
57  
58  
59  
60



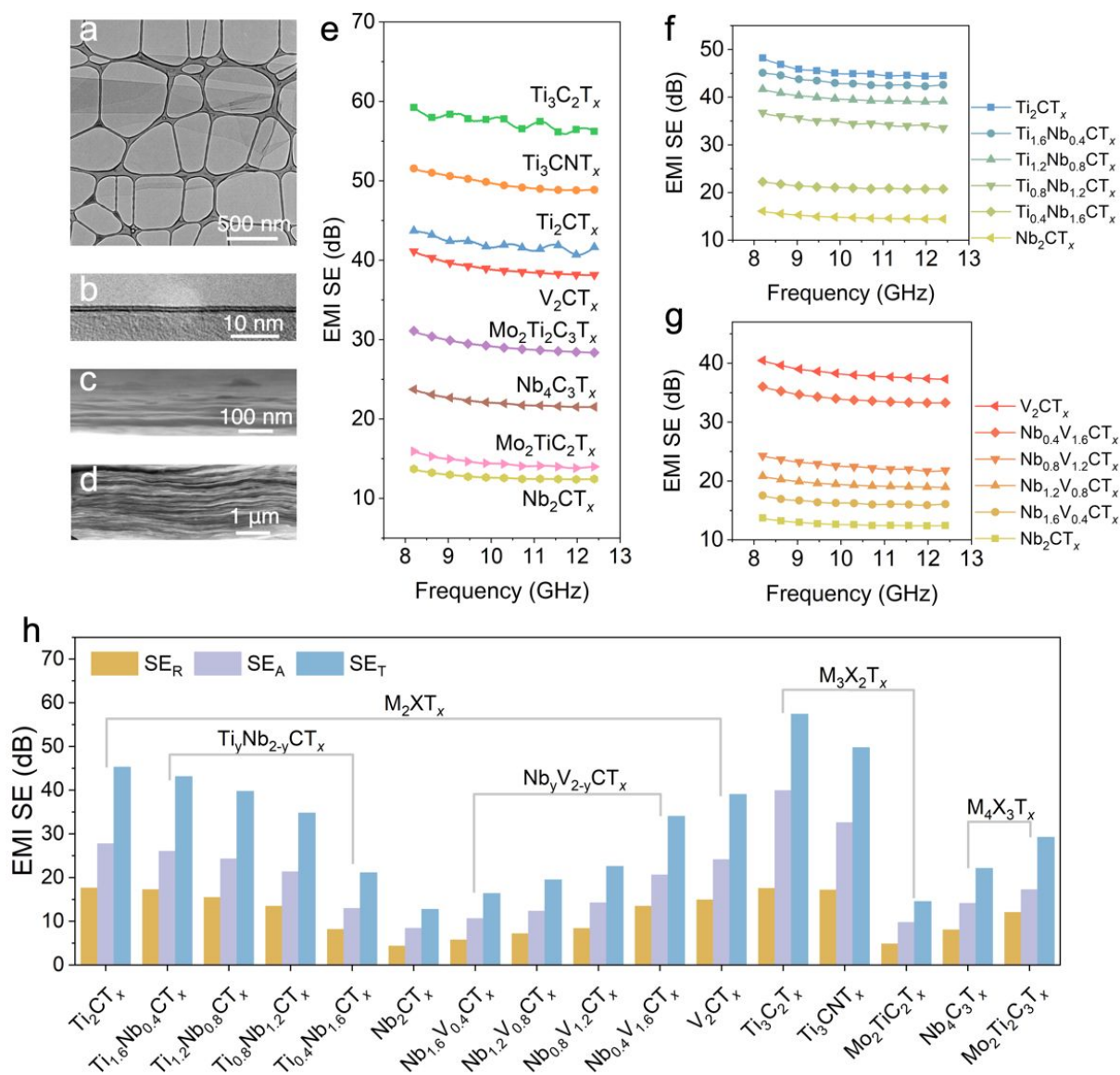


**Figure 2. Frequency-dependent EMI shielding performance of different MXenes.** (a) In-plane ([002] zone axis) TEM image of a typical MXene flake ( $\text{Ti}_2\text{CT}_x$  as an example). (b) TEM image of a double-layer MXene flake. (c) SEM image of the cross-section of a spray-coated  $\text{Ti}_2\text{CT}_x$  film on glass substrate showing an aligned layered structure. (d) SEM image of the cross-section of a vacuum-filtered freestanding  $\text{Ti}_2\text{CT}_x$  film showing the well-aligned layers. (e) EMI shielding effectiveness of different MXene ( $\text{M}_2\text{XT}_x$ ,  $\text{M}_3\text{X}_2\text{T}_x$  and  $\text{M}_4\text{X}_3\text{T}_x$ ) films ( $5 \pm 0.3 \mu\text{m}$  thick) in 8.2–12.4 GHz. EMI shielding effectiveness of solid solution (f)  $\text{Ti}_y\text{Nb}_{2-y}\text{CT}_x$  and (g)  $\text{Nb}_y\text{V}_{2-y}\text{CT}_x$  MXene films ( $5 \pm 0.3 \mu\text{m}$  thick), showing the controllable change of EMI SE with the chemistry. (h) The average EMI SE ( $\text{SE}_R$ ,  $\text{SE}_A$  and  $\text{SE}_T$ ) of different MXene films ( $5 \pm 0.3 \mu\text{m}$  thick) in 8.2–12.4 GHz, showing the reflection and absorption contributions.

1  
2  
3 (SE<sub>T</sub>, SE<sub>R</sub> and SE<sub>A</sub>) values in the X-band for different MXenes with a similar thickness ( $5 \pm 0.3$   
4  $\mu\text{m}$ ) is shown in Figure 2h. MXenes with higher SE<sub>T</sub> exhibit higher SE<sub>R</sub> and SE<sub>A</sub> values  
5  
6 simultaneously, indicating that MXenes with higher EMI shielding capability have a higher  
7  
8 contribution from EM wave reflection. Typically, the SE<sub>T</sub>, SE<sub>R</sub> and SE<sub>A</sub> values for Ti<sub>y</sub>Nb<sub>2-y</sub>CT<sub>x</sub>  
9  
10 and Nb<sub>y</sub>V<sub>2-y</sub>CT<sub>x</sub> decrease with increasing amounts of Nb. For M<sub>3</sub>X<sub>2</sub>T<sub>x</sub> MXenes, the average SE<sub>T</sub>,  
11  
12 SE<sub>R</sub> and SE<sub>A</sub> of Ti<sub>3</sub>C<sub>2</sub>T<sub>x</sub> reach 57.4 dB, 17.5 dB and 39.9 dB, respectively, while Ti<sub>3</sub>CNT<sub>x</sub> values  
13  
14 are 49.7 dB, 17 dB and 32.7 dB, respectively. We synthesized Ti<sub>3</sub>C<sub>2</sub>T<sub>x</sub> and Ti<sub>3</sub>CNT<sub>x</sub> using the  
15  
16 same etching (HF and HCl) and delamination (LiCl) methods. It suggests that the mono-X  
17  
18 MXene has better EMI shielding performance than the double-X MXene (carbonitride). For  
19  
20 ordered double-M MXene, Mo<sub>2</sub>TiC<sub>2</sub>T<sub>x</sub>, whose outer metal layers are Mo, shows a much lower  
21  
22 EMI shielding capability, in comparison with Ti<sub>3</sub>C<sub>2</sub>T<sub>x</sub>.  
23  
24  
25  
26  
27  
28

29  
30 Because EMI shielding properties are sensitive to the thickness of the shielding layers,  
31  
32 we measured the EMI shielding performance of all MXene films over a wide range of  
33  
34 thicknesses, and applied a model based on the transfer matrix method to validate them. Figure 3a  
35  
36 illustrates the continuum multi-layer structure with a plane EM wave (far-field) at normal  
37  
38 incidence to single MXene layers with interlayered free space (details of calculations are  
39  
40 presented in Supporting Information). Generally, Simon's formula is the most common approach  
41  
42 to verify the EMI shielding performance for highly conductive materials with thicknesses above  
43  
44 the skin depth ( $d \gg \delta$ ).<sup>27</sup> However, it is not applicable to nanometer- and submicrometer-thick  
45  
46 MXene films. The advantage of the transfer matrix modeling for ultrathin shielding layers,  
47  
48 compared to Simon's formula that neglects multiple reflection between the layers, is shown in  
49  
50 Figure S1. In absence of a model capturing the physics behind interactions of atomically thin  
51  
52 materials and EM waves<sup>28</sup>, this looks like the best option available today.  
53  
54  
55  
56  
57  
58  
59  
60

1  
2  
3 Figure 3b shows typical nanometer-thick  $\text{Ti}_3\text{C}_2\text{T}_x$  (dark green) and  $\text{Ti}_2\text{CT}_x$  (dark purple)  
4 films fabricated by spray-coating, and transparent single-layer MXene films that were spin-cast  
5 on glass substrates. The thickness of single-layer  $\text{Ti}_3\text{C}_2\text{T}_x$  and  $\text{Ti}_2\text{CT}_x$  flakes was measured using  
6 atomic force microscopy (AFM, Figure S6). The film thickness was calculated based on the  
7 transmittance and the absorption coefficients of  $\text{Ti}_3\text{C}_2\text{T}_x$  and  $\text{Ti}_2\text{CT}_x$  films at 550 nm wavelength  
8 (details in Figure S7).<sup>29,30</sup> The visible transmittance and color change with the increasing film  
9 thickness of  $\text{Ti}_3\text{C}_2\text{T}_x$  and  $\text{Ti}_2\text{CT}_x$  films are shown in Figure S8. Figure 3c shows the EMI  $\text{SE}_T$   
10 values of various nanometers-thick  $\text{Ti}_3\text{C}_2\text{T}_x$  and  $\text{Ti}_2\text{CT}_x$  films at 10 GHz. As the  $\text{Ti}_3\text{C}_2\text{T}_x$  films  
11 thickness increases from  $\sim 2$  nm to 137 nm, the  $\text{SE}_T$  value increases from 1.4 dB to 33 dB. It is  
12 highly significant that at  $\sim 40$  nm film thickness, the  $\text{SE}_T$  value reaches 21 dB, indicating that  
13 more than 99% of the EM waves have been intercepted. For  $\text{Ti}_2\text{CT}_x$  films, at 94 nm film  
14 thickness, the  $\text{SE}_T$  value reaches 13 dB, which is equivalent in shielding to a  $\sim 14$  nm-thick  
15  $\text{Ti}_3\text{C}_2\text{T}_x$  film. The gray line shows the simulated results using the transfer matrix model with the  
16 electrical conductivity. The modelling results agree sufficiently well with the experimental data.  
17 The  $\text{SE}_T$  values of  $\text{Ti}_3\text{C}_2\text{T}_x$  and  $\text{Ti}_2\text{CT}_x$  films decrease with the increasing frequency in the X-  
18 band (Figure S9a, b). Both  $\text{SE}_A$  and  $\text{SE}_R$  values increase with the increasing thickness (Figure  
19 S9c, d).

20  
21  
22 We further measured the total EMI SE values of all the vacuum-filtered MXene films  
23 with thicknesses ranging from  $\sim 1$  to 15  $\mu\text{m}$ . As shown in Figure 3d, the  $\text{SE}_T$  values of all the  
24 films show a nonlinear monotonic increase with the thickness, in fairly good agreement with the  
25 simulated results from the electrical conductivity values (gray line). This statistical result  
26 demonstrates that the transfer matrix model is more suitable for predicting the EMI shielding  
27 properties of thin films, as opposed to Simon's formula which predicts a linear relationship  
28  
29  
30  
31  
32  
33  
34  
35  
36  
37  
38  
39  
40  
41  
42  
43  
44  
45  
46  
47  
48  
49  
50  
51  
52  
53  
54  
55  
56  
57  
58  
59  
60

between thickness and EMI SE. Significantly, except  $\text{Nb}_2\text{CT}_x$ , all studied MXene films achieved  $\text{SE}_T > 20$  dB below  $10 \mu\text{m}$  thickness, including  $\text{M}_2\text{XT}_x$  ( $\text{Ti}_2\text{CT}_x$  and  $\text{V}_2\text{CT}_x$ ),  $\text{M}_3\text{X}_2\text{T}_x$  ( $\text{Ti}_3\text{C}_2\text{T}_x$ ,  $\text{Ti}_3\text{CNT}_x$  and  $\text{Mo}_2\text{TiC}_2\text{T}_x$ ), and  $\text{M}_4\text{X}_3\text{T}_x$  ( $\text{Nb}_4\text{C}_3\text{T}_x$  and  $\text{Mo}_2\text{Ti}_2\text{C}_3\text{T}_x$ ). In particular,  $\text{Ti}_3\text{C}_2\text{T}_x$ ,  $\text{Ti}_3\text{CNT}_x$ ,  $\text{Ti}_2\text{CT}_x$ ,  $\text{V}_2\text{CT}_x$  and  $\text{Mo}_2\text{Ti}_2\text{C}_3\text{T}_x$  films show  $\text{SE}_T > 20$  dB below  $2.5 \mu\text{m}$  film thickness. Compared to  $\text{Nb}_2\text{CT}_x$ ,  $\text{Nb}_4\text{C}_3\text{T}_x$  which has a similar elemental composition, shows a higher EMI SE at all film thicknesses. The same trend was found for  $\text{Ti}_2\text{CT}_x$  and  $\text{Ti}_3\text{C}_2\text{T}_x$ . It indicates that higher conductivity and EMI shielding can be obtained by increasing the number of layers in the

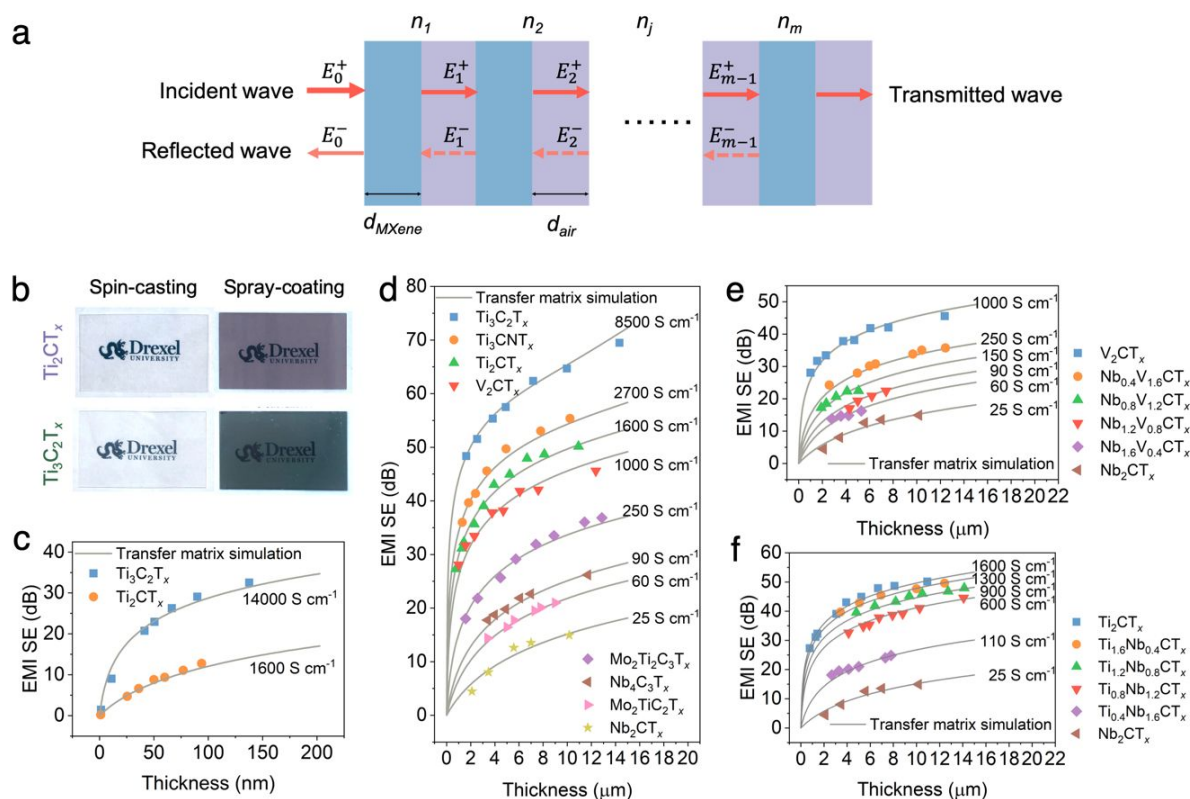


**Figure 3. Thickness-dependent EMI shielding performance of different MXenes.** (a) Schematic illustration for transfer matrix model simulating the interaction between the incident EM wave and MXene layers at normal incidence. (b) Digital images of spin-cast single-layer MXene films ( $\text{Ti}_3\text{C}_2\text{T}_x$  and  $\text{Ti}_2\text{CT}_x$ ), and spray-coated MXene films on glass substrates. (c) Simulated and experimental EMI SE values of spin-cast and spray-coated films ( $\text{Ti}_3\text{C}_2\text{T}_x$  and  $\text{Ti}_2\text{CT}_x$ ) with different thicknesses ( $<150$  nm) at 10 GHz. (d) Simulated and experimental EMI SE values of vacuum-filtered MXene ( $\text{M}_2\text{XT}_x$ ,  $\text{M}_3\text{X}_2\text{T}_x$  and  $\text{M}_4\text{X}_3\text{T}_x$ ) films with thicknesses from  $\sim 1$  to  $15 \mu\text{m}$  at 10 GHz. Simulated and experimental EMI SE values of solid solution (e)  $\text{Nb}_y\text{V}_{2-y}\text{CT}_x$  and (f)  $\text{Ti}_y\text{Nb}_{2-y}\text{CT}_x$  MXene films with different thicknesses at 10 GHz. The electrical conductivity values for the simulation are listed (c, d, e, and f).

1  
2  
3 MXene structure. The EMI shielding properties of two kinds of solid solution MXenes ( $\text{Nb}_y\text{V}_{2-y}\text{CT}_x$   
4 and  $\text{Ti}_y\text{Nb}_{2-y}\text{CT}_x$ ) were also measured and modeled at different thicknesses. Compared to  
5  
6 pure  $\text{Ti}_2\text{CT}_x$ ,  $\text{V}_2\text{CT}_x$  and  $\text{Nb}_2\text{CT}_x$ , the  $\text{SE}_T$  values of  $\text{Nb}_y\text{V}_{2-y}\text{CT}_x$  monotonically increase with the  
7  
8 V content, likewise with  $\text{Ti}_y\text{Nb}_{2-y}\text{CT}_x$  and Ti content (Figure 3e, f). Additionally, both show  
9  
10 excellent EMI shielding capabilities;  $\text{Ti}_y\text{Nb}_{2-y}\text{CT}_x$  and  $\text{Nb}_y\text{V}_{2-y}\text{CT}_x$  films can achieve  $\text{SE}_T > 20$   
11  
12 dB below 4  $\mu\text{m}$  and 8  $\mu\text{m}$  film thicknesses, respectively. This suggests that, in addition to  
13  
14  $\text{Ti}_3\text{C}_2\text{T}_x$ , many other MXenes can be used as thin EMI shielding coatings, although the  
15  
16 performance of  $\text{Ti}_3\text{C}_2\text{T}_x$  is still the best, possibly due to the optimized synthesis process that  
17  
18 minimized the concentration of defects and maximized the conductivity compared to initial  
19  
20 reports.<sup>13,14</sup> This is important as MXenes offer a variety of colors, mechanical, electrical and  
21  
22 other properties, enabling development of multifunctional EMI shielding films and coatings.  
23  
24 Furthermore, the EMI shielding performance is demonstrated to be tunable by control of the  
25  
26 chemistry of solid-solution MXenes over a broad range of thicknesses and compositions. The  
27  
28 frequency-dependent EMI SE values of all MXene films with different thicknesses can be found  
29  
30 in Figure S10. Notably, the electrical conductivity of the sprayed  $\text{Ti}_3\text{C}_2\text{T}_x$  films is  $\sim 14000 \text{ S cm}^{-1}$ ,  
31  
32 compared to the vacuum-filtered films ( $\sim 8500 \text{ S cm}^{-1}$ ). This is attributed to better alignment and  
33  
34 denser packing of MXene layers in the sprayed films (Figure S5).  
35  
36  
37  
38  
39  
40  
41  
42

43 To further understand the correlation between the electrical conductivity and EMI SE of  
44  
45 MXene films, we measured the electrical conductivity of all vacuum-filtered MXene films using  
46  
47 the four-point probe method. As shown in Figure 4a, Ti-based MXenes ( $\text{Ti}_3\text{C}_2\text{T}_x$ ,  $\text{Ti}_3\text{CNT}_x$ ,  
48  
49  $\text{Ti}_2\text{CT}_x$ , and  $\text{Ti}_{1.6}\text{Nb}_{0.4}\text{CT}_x$ ) along with  $\text{V}_2\text{CT}_x$ , exhibit electrical conductivity higher than  $1000 \text{ S}$   
50  
51  $\text{cm}^{-1}$ , while Nb-based MXenes have relatively low electrical conductivity. It is noteworthy that  
52  
53 the conductivity of MXenes varies with different synthesis processes and precursors. For the  
54  
55  
56  
57  
58  
59  
60

1  
2  
3 solid solution MXenes studied, the electrical conductivity of  $Ti_yNb_{2-y}CT_x$  and  $Nb_yV_{2-y}CT_x$  films  
4  
5 decreases with the increasing Nb content, consistent with the change of EMI shielding  
6  
7 performance. This indicates that both the electrical conductivity and EMI shielding capability of  
8  
9 MXenes are adjustable *via* their chemical composition.  
10  
11  
12

13 We further simulated the total EMI SE of MXene films with a thickness of 5  $\mu\text{m}$  using  
14  
15 the transfer matrix modeling at frequency of 10 GHz, and compared the modeled values to  
16  
17 experimentally measured electrical conductivity and  $SE_T$ . As shown in Figure 4b, for MXenes  
18  
19 with an electrical conductivity of  $> 100 \text{ S cm}^{-1}$ , the measured values are in close agreement with  
20  
21 the simulated results (gray line), showing a nonlinear increase of  $SE_T$  with the increasing  
22  
23 conductivity. However, for MXenes with an electrical conductivity of  $< 100 \text{ S cm}^{-1}$ , the  
24  
25 measured  $SE_T$  values are larger than predicted. This mismatch between the experimental results  
26  
27 and theoretical calculations implies that the electrical conductivity is not the only factor  
28  
29 responsible for EMI shielding performance of MXenes. On one hand, our theoretical calculations  
30  
31 using both the transfer matrix model and Simon's formula do not take into account dielectric  
32  
33 polarization effect. The dielectric interactions between the incident EM wave and MXene layers  
34  
35 are barely detected for those MXenes with higher conductivity, since the strong interaction  
36  
37 between abundant free electrons of highly conductive MXene and incident EM wave dominates  
38  
39 the shielding behavior. However, for MXenes with relatively low electrical conductivity, like  
40  
41  $Nb_2CT_x$ , the contribution of dielectric interactions between EM wave and the materials to EM  
42  
43 wave dissipation is not negligible. MXenes have abundant surface groups and point defects  
44  
45 caused by the acid-etching process, as well as adsorbed TMA ions between the layers.<sup>31,32</sup> They  
46  
47 may experience strong polarization accompanied with relaxation loss in the altered EM field,  
48  
49 contributing to EM wave absorption. On the other hand, both the transfer matrix model and  
50  
51  
52  
53  
54  
55  
56  
57  
58  
59  
60

Simon's formula do not take into account the difference between AC conductivity and DC conductivity for MXenes in the X-band. The frequency-dependent conductivity behavior of different MXenes at gigahertz frequencies is not known, although AC conductivity usually asymptotically approaches the DC conductivity for metals and carbon materials.<sup>33-35</sup> Further investigation is required to quantify the dielectric properties and AC conductivities of MXenes for better understanding of the interaction between EM waves and MXenes. Also, physical models accounting for nanometer-scale heterogeneity of assembled MXene films should be developed.

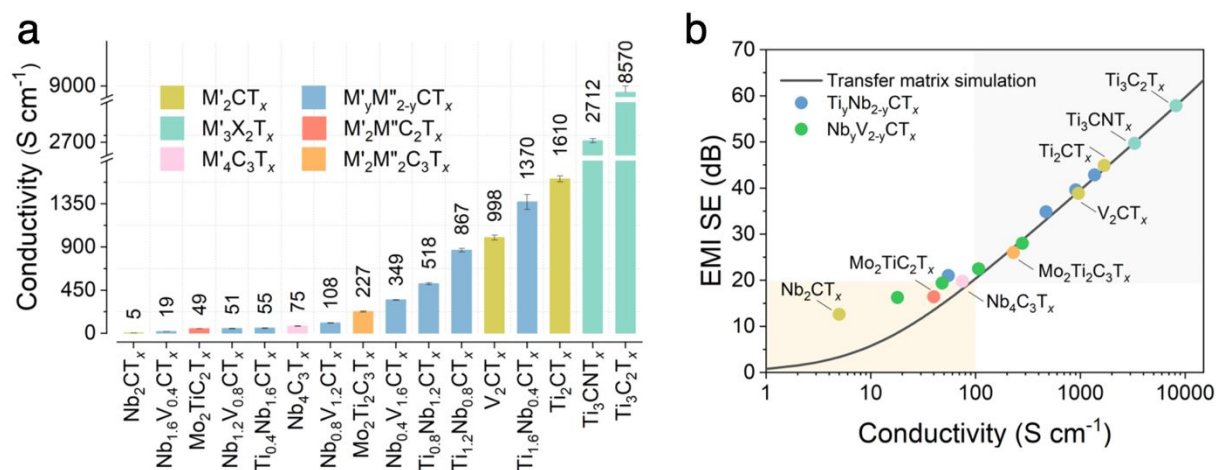


**Figure 4. Conductivity-dependent EMI shielding performance of different MXenes.** (a) The electrical conductivity of different MXene films. (b) Comparison of EMI SE values between transfer matrix simulation and as-prepared MXene films with a thickness of  $\sim 5 \mu\text{m}$  at 10 GHz, showing the relationship between EMI SE and the electrical conductivity of MXenes.

We have summarized the progress of metal-based hybrids and carbon materials for EMI shielding in recent years, and highlighted the characteristic interval for the MXene films with  $\sim 2$  nm to  $15 \mu\text{m}$  thickness based on the measured EMI shielding properties of different MXenes (details in Table S3). As depicted in Figure 5, it is apparent that most metal-based hybrids and carbon materials require characteristic layer thickness of  $\sim 0.1$ - $3$  mm to achieve useful EMI SE



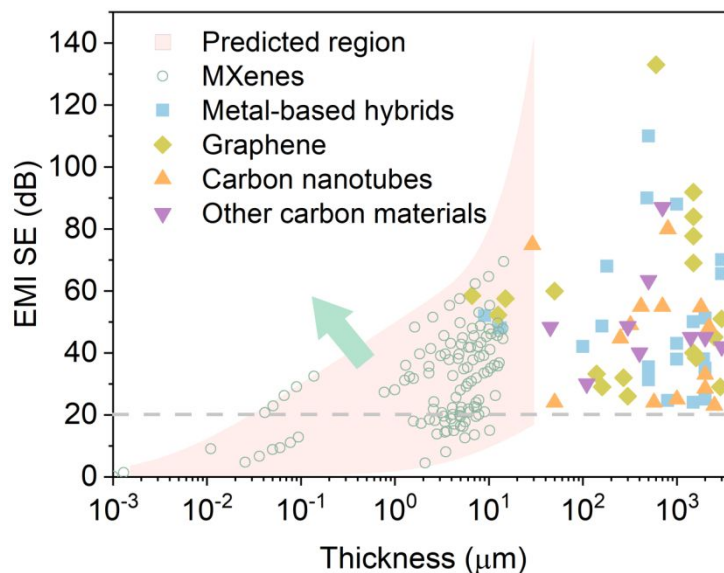


**Figure 5. Performance of different materials towards EMI shielding.** A comparison of the total EMI SE thickness for the MXene family with metal-based hybrids and carbon materials (graphene, carbon nanotubes, carbon fibers, and others). The gray dashed line is the baseline for the commercial EMI shielding materials ( $SE_T > 20$  dB). A direct comparison of the electrical conductivity and EMI shielding properties of different MXenes with other materials from the literature over the last five years can be found in Table S3.

values, even though some progress has been made in developing thin shielding layers using graphene and metal-based hybrids.<sup>36,37</sup> By contrast, MXenes are effective EMI shields over a broad range of thicknesses, with a minimum thickness of only  $\sim 40$  nm sufficient to achieve 20 dB EMI SE. Furthermore, higher EMI shielding performance can be obtained through further optimization of MAX phase and MXene synthesis, and through modification of the surface chemistry. Many of the MXenes studied in this work were not even previously reported and no optimization of synthesis and conductivity has been done for majority of materials in this study. MXenes not only show superiority with respect to thickness and the feasibility of different coating techniques, but also offer a variety of candidates for manufacturing multifunctional EMI shielding coatings coupled with the optical, mechanical and other properties of different MXenes. It is promising for design of gradient multilayers with tunable EMI shielding properties



1  
2  
3 using the various combinations of different MXenes. More broadly, the fact that numerous  
4  
5 MXenes with different compositions and structures are still unexplored shows the possibility to  
6  
7 extend the EMI shielding interval of MXenes towards higher EMI shielding effectiveness and  
8  
9 thinner layers.  
10  
11  
12  
13  
14  
15

## 16 CONCLUSIONS

17  
18  
19 In summary, sixteen MXenes with different compositions and  $M_2X_2T_x$ ,  $M_3X_2T_x$  and  
20  
21  $M_4X_3T_x$  structures have been synthesized, delaminated and used to make films of varying  
22  
23 thickness. This is the largest set of MXene compositions compared in any single study to date,  
24  
25 which demonstrates a wide variety of MXene properties and ways to control them. These  
26  
27 samples offer an insight into effects of structure and composition on properties of MXenes. We  
28  
29 have showed that the investigated MXene films, ranging from 40 nanometers to several  
30  
31 micrometers in thickness, are promising as thin EMI shielding coatings. A transfer matrix model  
32  
33 has been shown to fit the EMI shielding performance of MXenes, at least for the most  
34  
35 conducting members of the MXene family. Since MXenes have wide variety of useful  
36  
37 properties, these results also build a platform for developing multifunctional materials with  
38  
39 tunable EMI shielding properties using various MXenes.  
40  
41  
42  
43  
44  
45  
46  
47  
48

## 49 METHODS

50  
51  
52 **Materials.** For synthesis of the MAX phase precursors, Ti (99.5%, -325 mesh, Alfa  
53  
54 Aesar), Al (99.5%, -325 mesh, Alfa Aesar), V (99.5%, -325 mesh, Alfa Aesar), Nb (99.99%, -  
55  
56  
57  
58  
59  
60

1  
2  
3 325 mesh, Beantown Chemical), AlN (98%, 10  $\mu\text{m}$ , Aldrich), C (graphite, 99%, -325 mesh, Alfa  
4 Aesar), TiC (99.5%, typically 2  $\mu\text{m}$ , Alfa Aesar), and Mo (99.9%, -250 mesh, Alfa Aesar)  
5  
6 powders were used. For topochemical synthesis to MXene, hydrochloric acid (HCl, 36.5-38%,  
7 Fisher Chemical), hydrofluoric acid (HF, 48.5-51%, Acros Organics), lithium chloride (LiCl,  
8 99%, Acros Organics), lithium fluoride (LiF, 98.5%, Alfa Aesar), tetramethylammonium  
9 hydroxide (TMAOH, 25 wt%, Acros Organics) were used directly without further purification.

10  
11  
12  
13  
14  
15  
16  
17  
18 **Synthesis of MAX powders.** Prior to synthesis, all precursor powders (Table S1,  
19 Supporting Information) were mixed with 10 mm zirconia balls in a 2:1 ball : powder ratio. The  
20 mixture was placed into plastic jars, then ball milled at 50 rpm for 18 hours. The powder mixture  
21 was then transferred to alumina crucibles, which were placed into a high temperature furnace  
22 (Carbolite Gero). Ar was flowed through the furnace for 1 h prior to heating, then was  
23 continually flowed through the furnace during synthesis. For all samples, the heating rate was 3  
24  $^{\circ}\text{C min}^{-1}$ . Depending on the chemistry and composition, different temperatures and holding times  
25 were used (details in Table S1). After cooling, the samples were milled using a TiN-coated  
26 milling bit, then were sieved to  $<75 \mu\text{m}$ .

27  
28  
29  
30  
31  
32  
33  
34  
35  
36  
37  
38  
39 **Synthesis of MXenes.** The synthesis conditions of sixteen MXenes are summarized in  
40 Table S2 in Supporting Information. The synthesized procedures in detail for different MXenes  
41 are as follows.

42  
43  
44  
45  
46  
47 *Synthesis of  $\text{Ti}_3\text{C}_2\text{T}_x$ ,  $\text{Ti}_2\text{CT}_x$  and  $\text{Ti}_3\text{CNT}_x$ .*  $\text{Ti}_3\text{C}_2\text{T}_x$ ,  $\text{Ti}_2\text{CT}_x$  and  $\text{Ti}_3\text{CNT}_x$  were  
48 synthesized by the selective etching of the corresponding MAX phase powders ( $\text{Ti}_3\text{AlC}_2$ ,  $\text{Ti}_2\text{AlC}$   
49 and  $\text{Ti}_3\text{AlCN}$ ) with HF and HCl. Typically, 12 mL of HCl, 2 mL of HF and 6 mL of deionized  
50 (DI) water were mixed firstly. After that, 1 g of MAX powder was added to the solution, and  
51  
52  
53  
54  
55  
56  
57  
58  
59  
60

1  
2  
3 then the mixture kept stirring for 24 h at room temperature. After the etching is done, the reacted  
4 solution was centrifuged at 3500 rpm for 2 mins. This washing process was repeated until pH  
5 value is >6. The centrifuged sediment was added into a solution of LiCl in DI water with a  
6 concentration of 20 mg mL<sup>-1</sup>. The mixture was stirred for 4 h at room temperature. After that, the  
7 solution was centrifuged at 3500 rpm for 10 mins. The centrifugation was repeated until the  
8 supernatant became black. The black solution was collected and centrifuged at 7500 rpm for 3  
9 mins. The final supernatant was used for the preparation of MXene films.

10  
11  
12  
13  
14  
15  
16  
17  
18  
19  
20 *Synthesis of Mo<sub>2</sub>TiC<sub>2</sub>T<sub>x</sub> and Mo<sub>2</sub>Ti<sub>2</sub>C<sub>3</sub>T<sub>x</sub> and Nb<sub>4</sub>C<sub>3</sub>T<sub>x</sub>.* Mo<sub>2</sub>TiC<sub>2</sub>T<sub>x</sub> and Mo<sub>2</sub>Ti<sub>2</sub>C<sub>3</sub>T<sub>x</sub> and  
21 Nb<sub>4</sub>C<sub>3</sub>T<sub>x</sub> were synthesized by the selective etching of the corresponding MAX phase powders  
22 (Mo<sub>2</sub>TiAlC<sub>2</sub>, Mo<sub>2</sub>Ti<sub>2</sub>AlC<sub>3</sub> and Nb<sub>4</sub>AlC<sub>3</sub>) with HF. Typically, 1 g of MAX phase powder was  
23 added into 20 mL of HF with stirring at 50 °C. The etching time for Mo<sub>2</sub>TiAlC<sub>2</sub>, Mo<sub>2</sub>Ti<sub>2</sub>AlC<sub>3</sub>  
24 and Nb<sub>4</sub>AlC<sub>3</sub> was 48 h, 96 h and 7 days, respectively. After etching, the reacted solution was  
25 washed with DI water through centrifugation (3500 rpm, 2 mins) several times until the pH value  
26 is >6. After that, the centrifuged sediment was added into a solution with 0.5 g of TMAOH and  
27 20 mL of DI water, and stirred for 12 h at room temperature. The mixture was centrifuged  
28 several times with DI water at 9000 rpm for 10 mins until the pH value is <8. At last, the  
29 solution was centrifuged at 3500 rpm for 10 mins. The black supernatant was the dispersion of  
30 delaminated MXene flakes in water.

31  
32  
33  
34  
35  
36  
37  
38  
39  
40  
41  
42  
43  
44  
45  
46 *Synthesis of Ti<sub>y</sub>Nb<sub>2-y</sub>CT<sub>x</sub>.* Ti<sub>y</sub>Nb<sub>2-y</sub>CT<sub>x</sub> (y= 0.4, 0.8, 1.2 and 1.6) was synthesized by the  
47 selective etching of Ti<sub>y</sub>Nb<sub>2-y</sub>AlC powders with a mild method (LiF + HCl). Typically, LiF was  
48 dissolved in a mixture of 5mL of DI water and 15 mL of HCl. After that, 1 g of Ti<sub>y</sub>Nb<sub>2-y</sub>AlC  
49 powder was added to the etchant solution gradually, and stirred for 48 h at 35 °C. Following the  
50 reaction, the solution was centrifuged with DI water at 3500 rpm for 2 mins. This washing  
51  
52  
53  
54  
55  
56  
57  
58  
59  
60

1  
2  
3 procedure was repeated several times until the pH was >6. Finally, the delaminated  $\text{Ti}_y\text{Nb}_{2-y}\text{CT}_x$   
4  
5 was obtained when the stable black dispersion formed. The supernatant was attained by  
6  
7 centrifugation at 7500 rpm for 3 min.  
8  
9

10  
11 *Synthesis of  $\text{Nb}_y\text{V}_{2-y}\text{CT}_x$ .*  $\text{Nb}_y\text{V}_{2-y}\text{CT}_x$  ( $y= 0, 0.4, 0.8, 1.2, 1.6$  and  $2$ ) was synthesized by  
12  
13 the selective etching of the corresponding  $\text{Nb}_y\text{V}_{2-y}\text{AlC}$  powders with HF. The etching and  
14  
15 delaminated processes are the same as those of  $\text{Mo}_2\text{TiC}_2\text{T}_x$  except the etching temperature is 35  
16  
17 °C.  
18  
19

20  
21 **Fabrication of MXene films.** The glass slides ( $24 \times 40 \times 0.13$  mm, Corning, USA) were  
22  
23 used as the substrate for spin-casting and spray-coating. Before depositing MXene flakes, the  
24  
25 substrates were cleaned with a bath sonication in ethanol and DI water sequentially, and then  
26  
27 dried with compressed air. After that, the substrates were cleaned by oxygen plasma with a  
28  
29 power of 100 W for 5 mins at a gas flow of 3 sccm.  
30  
31

32  
33 *Spin-casting.* The ~2 nm thick MXene films ( $\text{Ti}_3\text{C}_2\text{T}_x$  and  $\text{Ti}_2\text{CT}_x$ ) were prepared using  
34  
35 spin-casting method. Typically, the colloidal solution with a concentration of  $1 \text{ mg mL}^{-1}$  was  
36  
37 spin-cast onto the substrate with spin rate of 1000 rpm for 30 s, followed by 5000 rpm for 10 s.  
38  
39

40  
41 *Spray-coating.* The MXene films ( $\text{Ti}_3\text{C}_2\text{T}_x$  and  $\text{Ti}_2\text{CT}_x$ ) with the thickness of <150 nm  
42  
43 were prepared using spray-coating method. Typically, the colloidal solution with a concentration  
44  
45 of  $1 \text{ mg mL}^{-1}$  was sprayed onto the substrate manually. The spray flow was controlled to avoid  
46  
47 droplets agglomerating on the substrate. Air flow from a dryer above the substrate provided  
48  
49 sufficiently fast drying after each spray.  
50  
51

52  
53 *Vacuum-assistant filtration.* The freestanding MXene films were prepared by vacuum-  
54  
55 filtering the colloidal MXene dispersion on a polypropylene film with a thickness of 25  $\mu\text{m}$   
56  
57  
58  
59  
60

1  
2  
3 (3501 Coated PP, Celgard LLC), and followed by drying in vacuum. The concentration of the  
4 colloidal MXene dispersion was calculated based on the weight of the film and the filtered  
5 volume of the dispersion.  
6  
7  
8  
9

10 All films were dried in vacuum oven at 70 °C for 12 h before testing.  
11  
12

13  
14 **Characterization.** The morphology and structure of MXene flakes and films were  
15 observed using a 3D laser scanning confocal microscopy (Keyence, VK-X1000, Japan), scanning  
16 electron microscopy (SEM; Zeiss Supra 50VP, Germany) and transmission electron microscopy  
17 (TEM; F-30, FEI-Tecnai, USA). The thickness of MXene flakes was measured by atomic force  
18 microscopy (AFM; Multimode 8, Bruker, USA) with a Si tip (Budget Sensors Tap300Al-G;  $f_0 =$   
19 300 kHz,  $k = 40 \text{ N m}^{-1}$ ) in a standard tapping mode in air. X-ray diffraction (XRD) patterns were  
20 recorded with Ni-filtered Cu K $\alpha$  radiation ( $\lambda = 1.54 \text{ \AA}$ ; Miniflex, Rigaku, USA) operated at 40  
21 kV and 15 mA. The electrical conductivity of MXene films was measured by a four-point probe  
22 instrument (ResTest, Jandel Engineering Ltd., Bedfordshire, U.K.) with a probe distance of 1  
23 mm. The thickness of vacuum-filtrated films was measured by a micrometer with 0.1  $\mu\text{m}$   
24 accuracy. UV–vis spectroscopy was performed from 300 to 1000 nm (Evolution 201, Thermo  
25 Scientific, 10 mm path length quartz cuvette, USA), and the transmittance value at 550 nm was  
26 used to quantify the thickness of the spin-cast and spray-coated films. Scattering parameters of  
27 the films were measured using a vector network analyzer (8720ES, Agilent, USA) with a WR-90  
28 rectangular waveguide in the frequency range of 8.2–12.4 GHz.  
29  
30  
31  
32  
33  
34  
35  
36  
37  
38  
39  
40  
41  
42  
43  
44  
45  
46  
47  
48  
49  
50  
51

## 52 AUTHOR INFORMATION

### 53 54 55 **Corresponding Author** 56 57 58 59 60

1  
2  
3 \* Prof. Yury Gogotsi (Y. G.), E-mail: gogotsi@drexel.edu.  
4  
5

## 6 **ORCID**

7

8  
9 Meikang Han: 0000-0003-3309-988X

10  
11 Christopher Eugene Shuck: 0000-0002-1274-8484

12  
13 Babak Anasori: 0000-0002-1955-253X

14  
15 Chong Min Koo: 0000-0002-8674-9236

16  
17 Yury Gogotsi: 0000-0001-9423-4032  
18  
19

## 20 **Author Contributions**

21

22  
23 M. H., D. P. and R. R. synthesized MXenes and fabricated MXene films. C. S. and B. A.  
24 synthesized MAX phases. M. H. performed the electromagnetic measurement and analyzed the  
25 data. G. F. and C. K. contributed to the prediction modelling. M. H. wrote the manuscript, with  
26 input from all co-authors. Y. G. initiated the study and supervised the work.  
27  
28  
29  
30  
31  
32

## 33 **ACKNOWLEDGEMENTS**

34

35  
36 We thank Dr. Narendra Kurra, Dr. Xu Xiao, and Dr. Mikhail Shekhirev for the MXene film  
37 morphology studies, as well as Mark Anayee for computer programming. We are grateful to  
38 Murata Manufacturing Co., Ltd, Japan, for providing equipment used for testing EMI shielding  
39 properties of MXenes. C. K. acknowledges the financial support from the National Research  
40 Foundation of Korea (2017R1A2B3006469 and 2019M3D1A2014004).  
41  
42  
43  
44  
45  
46  
47  
48

## 49 **SUPPORTING INFORMATION**

50

51  
52 The Supporting Information is available free of charge at <https://pubs.acs.org>.  
53  
54  
55  
56  
57  
58  
59  
60

1  
2  
3 Additional experimental conditions and results, including the tables of synthesis conditions for  
4 MAX phases and MXenes; Transfer matrix modeling; XRD patterns of MAX phases and  
5 MXenes; Surface morphologies of MXene films; AFM images of MXene flakes; The thickness  
6 calculation of MXene films, and corresponding UV-VIS spectra; EMI SE of all MXene films.  
7  
8 Table on the comparison of EMI shielding performance of various materials.  
9  
10  
11  
12  
13

## 14 REFERENCES

- 15  
16  
17  
18 (1) Médard, M., Is 5 Just What Comes after 4? *Nat. Electron.* **2020**, *3*, 2-4.  
19  
20  
21 (2) Huang, W.; Zhou, J.; Froeter, P. J.; Walsh, K.; Liu, S.; Kraman, M. D.; Li, M.;  
22 Michaels, J. A.; Sievers, D. J.; Gong, S.; Li, X., Three-Dimensional Radio-Frequency  
23 Transformers Based on a Self-Rolled-Up Membrane Platform. *Nat. Electron.* **2018**, *1*, 305-313.  
24  
25  
26 (3) Jiang, Z. Y.; Huang, W.; Chen, L. S.; Liu, Y. H., Ultrathin, Lightweight, and  
27 Freestanding Metallic Mesh for Transparent Electromagnetic Interference Shielding. *Opt.*  
28 *Express* **2019**, *27*, 24194-24206.  
29  
30  
31 (4) Wan, Y. J.; Zhu, P. L.; Yu, S. H.; Sun, R.; Wong, C. P.; Liao, W. H., Anticorrosive,  
32 Ultralight, and Flexible Carbon-Wrapped Metallic Nanowire Hybrid Sponges for Highly  
33 Efficient Electromagnetic Interference Shielding. *Small* **2018**, *14*, 1800534.  
34  
35  
36 (5) Chung, D. D. L., Materials for Electromagnetic Interference Shielding. *J. Mater. Eng.*  
37 *Perform.* **2000**, *9*, 350-354.  
38  
39  
40 (6) Chen, Z.; Xu, C.; Ma, C.; Ren, W.; Cheng, H. M., Lightweight and Flexible Graphene  
41 Foam Composites for High-Performance Electromagnetic Interference Shielding. *Adv. Mater.*  
42 **2013**, *25*, 1296-1300.  
43  
44  
45  
46  
47  
48  
49  
50  
51  
52  
53  
54  
55  
56  
57  
58  
59  
60

1  
2  
3 (7) Wei, Q.; Pei, S.; Qian, X.; Liu, H.; Liu, Z.; Zhang, W.; Zhou, T.; Zhang, Z.; Zhang,  
4 X.; Cheng, H. M.; Ren, W., Superhigh Electromagnetic Interference Shielding of Ultrathin  
5 Aligned Pristine Graphene Nanosheets Film. *Adv. Mater.* DOI: 10.1002/adma.201907411.  
6  
7

8  
9  
10 (8) Shahzad, F.; Alhabeab, M.; Hatter, C. B.; Anasori, B.; Hong, S. M.; Koo, C. M.;  
11 Gogotsi, Y., Electromagnetic Interference Shielding with 2D Transition Metal Carbides  
12 (MXenes). *Science* **2016**, *353*, 1137-1140.  
13  
14  
15

16  
17 (9) Han, M.; Yin, X.; Hantanasirisakul, K.; Li, X.; Iqbal, A.; Hatter, C. B.; Anasori, B.;  
18 Koo, C. M.; Torita, T.; Soda, Y.; Zhang, L.; Cheng, L.; Gogotsi, Y., Anisotropic MXene  
19 Aerogels with a Mechanically Tunable Ratio of Electromagnetic Wave Reflection to Absorption.  
20  
21  
22  
23  
24  
25  
26  
27  
28  
29  
30  
31  
32  
33  
34  
35  
36  
37  
38  
39  
40  
41  
42  
43  
44  
45  
46  
47  
48  
49  
50  
51  
52  
53  
54  
55  
56  
57  
58  
59  
60

(10) Yun, T.; Kim, H.; Iqbal, A.; Cho, Y. S.; Lee, G. S.; Kim, M. K.; Kim, S. J.; Kim, D.;  
Gogotsi, Y.; Kim, S. O., Electromagnetic Shielding of Monolayer MXene Assemblies. *Adv.*  
*Mater.*, **2020**, *32*, 2070064.

(11) Wu, X.; Han, B.; Zhang, H. B.; Xie, X.; Tu, T.; Zhang, Y.; Dai, Y.; Yang, R.; Yu, Z.  
Z., Compressible, Durable and Conductive Polydimethylsiloxane-Coated MXene Foams for  
High-Performance Electromagnetic Interference Shielding. *Chem. Eng. J.* **2020**, *381*, 122622.

(12) Liu, J.; Zhang, H. B.; Sun, R.; Liu, Y.; Liu, Z.; Zhou, A.; Yu, Z. Z., Hydrophobic,  
Flexible, and Lightweight MXene Foams for High-Performance Electromagnetic Interference  
Shielding. *Adv. Mater.* **2017**, *29*, 1702367.

(13) Zhao, S.; Zhang, H. B.; Luo, J. Q.; Wang, Q. W.; Xu, B.; Hong, S.; Yu, Z. Z., Highly  
Electrically Conductive Three-Dimensional  $\text{Ti}_3\text{C}_2\text{T}_x$  MXene/Reduced Graphene Oxide Hybrid



1  
2  
3 Aerogels with Excellent Electromagnetic Interference Shielding Performances. *ACS Nano* **2018**,  
4 *12*, 11193-11202.

5  
6  
7  
8 (14) Weng, G. M.; Li, J.; Alhabeab, M.; Karpovich, C.; Wang, H.; Lipton, J.; Maleski, K.;  
9 Kong, J.; Shaulsky, E.; Elimelech, M.; Gogotsi, Y.; Taylor, A. D., Layer-by-Layer Assembly  
10 of Cross-Functional Semi-Transparent MXene-Carbon Nanotubes Composite Films for Next-  
11 Generation Electromagnetic Interference Shielding. *Adv. Funct. Mater.* **2018**, *28*, 1803360.

12  
13  
14  
15 (15) Zhang, C. J.; McKeon, L.; Kremer, M. P.; Park, S. H.; Ronan, O.; Seral Ascaso, A.;  
16 Barwich, S.; Coileáin, C. Ó.; McEvoy, N.; Nerl, H. C., Additive-Free MXene Inks and Direct  
17 Printing of Micro-Supercapacitors. *Nat. Commun.* **2019**, *10*, 1795.

18  
19  
20  
21 (16) Sarycheva, A.; Polemi, A.; Liu, Y.; Dandekar, K.; Anasori, B.; Gogotsi, Y., 2D  
22 Titanium Carbide (MXene) for Wireless Communication. *Sci. Adv.* **2018**, *4*, eaau0920.

23  
24  
25  
26 (17) Salles, P.; Pinto, D.; Hantanasirisakul, K.; Maleski, K.; Shuck, C. E.; Gogotsi, Y.,  
27 Electrochromic Effect in Titanium Carbide MXene Thin Films Produced by Dip-Coating. *Adv.*  
28 *Funct. Mater.* **2019**, *29*, 1809223.

29  
30  
31  
32 (18) Kim, S. J.; Choi, J.; Maleski, K.; Hantanasirisakul, K.; Jung, H. T.; Gogotsi, Y.; Ahn,  
33 C. W., Interfacial Assembly of Ultrathin, Functional MXene Films. *ACS Appl. Mater. Interfaces*  
34 **2019**, *11*, 32320-32327.

35  
36  
37  
38 (19) Anasori, B.; Lukatskaya, M. R.; Gogotsi, Y., 2D Metal Carbides and Nitrides (MXenes)  
39 for Energy Storage. *Nat. Rev. Mater.* **2017**, *2*, 16098.

40  
41  
42  
43 (20) Deysher, G.; Shuck, C. E.; Hantanasirisakul, K.; Frey, N. C.; Foucher, A. C.; Maleski,  
44 K.; Sarycheva, A.; Shenoy, V. B.; Stach, E. A.; Anasori, B.; Gogotsi, Y., Synthesis of  
45  
46  
47  
48  
49  
50  
51  
52  
53  
54  
55  
56  
57  
58  
59  
60

1  
2  
3 Mo<sub>4</sub>VAI<sub>4</sub>C<sub>4</sub> MAX Phase and Two-Dimensional Mo<sub>4</sub>VC<sub>4</sub> MXene with 5 Atomic Layers of  
4  
5 Transition Metals. *ACS Nano* **2020**, *14*, 204-217.  
6  
7

8 (21) Sokol, M.; Natu, V.; Kota, S.; Barsoum, M. W., On the Chemical Diversity of the MAX  
9 Phases. *Trends Chem.* **2019**, *1*, 210-223.  
10  
11

12 (22) Anasori, B.; Gogotsi, Y., *2D Metal Carbides and Nitrides (MXenes)*. Springer: Berlin,  
13 **2019**; pp 15-19.  
14  
15

16 (23) Maleski, K.; Mochalin, V. N.; Gogotsi, Y., Dispersions of Two-Dimensional Titanium  
17 Carbide MXene in Organic Solvents. *Chem. Mater.* **2017**, *29*, 1632-1640.  
18  
19

20 (24) Hantanasirisakul, K.; Gogotsi, Y., Electronic and Optical Properties of 2D Transition  
21 Metal Carbides and Nitrides (MXenes). *Adv. Mater.* **2018**, *30*, 1804779.  
22  
23

24 (25) Anasori, B.; Xie, Y.; Beidaghi, M.; Lu, J.; Hosler, B. C.; Hultman, L.; Kent, P. R. C.;  
25 Gogotsi, Y.; Barsoum, M. W., Two-Dimensional, Ordered, Double Transition Metals Carbides  
26 (MXenes). *ACS Nano* **2015**, *9*, 9507-9516.  
27  
28

29 (26) Seredych, M.; Shuck, C. E.; Pinto, D.; Alhabeab, M.; Precetti, E.; Deysner, G.;  
30 Anasori, B.; Kurra, N.; Gogotsi, Y., High-Temperature Behavior and Surface Chemistry of  
31 Carbide MXenes Studied by Thermal Analysis. *Chem. Mater.* **2019**, *31*, 3324-3332.  
32  
33

34 (27) Simon, R. M., EMI Shielding through Conductive Plastics. *Polym. Plast. Technol. Eng.*  
35 **1981**, *17*, 1-10.  
36  
37

38 (28) Yang, Y.; Zhu, D.; Yan, W.; Agarwal, A.; Zheng, M.; Joannopoulos, J. D.; Lalanne,  
39 P.; Christensen, T.; Berggren, K. K.; Soljačić, M., A General Theoretical and Experimental  
40 Framework for Nanoscale Electromagnetism. *Nature* **2019**, *576*, 248-252.  
41  
42  
43  
44  
45  
46  
47  
48  
49  
50

1  
2  
3 (29) Dillon, A. D.; Ghidui, M. J.; Krick, A. L.; Griggs, J.; May, S. J.; Gogotsi, Y.;  
4 Barsoum, M. W.; Fafarman, A. T., Highly Conductive Optical Quality Solution-Processed Films  
5 of 2D Titanium Carbide. *Adv. Funct. Mater.* **2016**, *26*, 4162-4168.  
6  
7

8  
9  
10 (30) Ying, G.; Dillon, A. D.; Fafarman, A. T.; Barsoum, M. W., Transparent, Conductive  
11 Solution Processed Spincoated 2D Ti<sub>2</sub>CT<sub>x</sub> (MXene) Films. *Mater. Res. Lett.* **2017**, *5*, 391-398.  
12  
13

14  
15 (31) Watts, P. C. P.; Hsu, W. K.; Barnes, A.; Chambers, B., High Permittivity from  
16 Defective Multiwalled Carbon Nanotubes in the X-Band. *Adv. Mater.* **2003**, *15*, 600-603.  
17  
18

19  
20 (32) Yin, X.; Kong, L.; Zhang, L.; Cheng, L.; Travitzky, N.; Greil, P., Electromagnetic  
21 Properties of Si-C-N Based Ceramics and Composites. *Int. Mater. Rev.* **2014**, *59*, 326-355.  
22  
23

24  
25 (33) Al-Saleh, M. H.; Saadeh, W. H.; Sundararaj, U., EMI Shielding Effectiveness of Carbon  
26 Based Nanostructured Polymeric Materials: A Comparative Study. *Carbon* **2013**, *60*, 146-156.  
27  
28

29  
30 (34) Naishadham, K.; Kadaba, P. K., Measurement of the Microwave Conductivity of a  
31 Polymeric Material with Potential Applications in Absorbers and Shielding. *IEEE Trans.*  
32 *Microw. Theory Tech.* **1991**, *39*, 1158-1164.  
33  
34

35  
36 (35) Awan, S.; Lombardo, A.; Colli, A.; Privitera, G.; Kulmala, T.; Kivioja, J.; Koshino,  
37 M.; Ferrari, A., Transport Conductivity of Graphene at RF and Microwave Frequencies. *2D*  
38 *Mater.* **2016**, *3*, 015010.  
39  
40

41  
42 (36) Wang, Z.; Mao, B.; Wang, Q.; Yu, J.; Dai, J.; Song, R.; Pu, Z.; He, D.; Wu, Z.; Mu,  
43 S., Ultrahigh Conductive Copper/Large Flake Size Graphene Heterostructure Thin Film with  
44 Remarkable Electromagnetic Interference Shielding Effectiveness. *Small* **2018**, *14*, 1704332.  
45  
46  
47  
48  
49  
50  
51  
52  
53  
54  
55  
56  
57  
58  
59  
60

1  
2  
3 (37) Lin, S.; Ju, S.; Shi, G.; Zhang, J.; He, Y.; Jiang, D., Ultrathin Nitrogen-Doping  
4 Graphene Films for Flexible and Stretchable EMI Shielding Materials. *J. Mater. Sci.* **2019**, *54*,  
5  
6 7165-7179.  
7  
8  
9  
10  
11  
12  
13  
14  
15  
16  
17  
18  
19  
20  
21  
22  
23  
24  
25  
26  
27  
28  
29  
30  
31  
32  
33  
34  
35  
36  
37  
38  
39  
40  
41  
42  
43  
44  
45  
46  
47  
48  
49  
50  
51  
52  
53  
54  
55  
56  
57  
58  
59  
60

## TABLE OF CONTENTS GRAPHIC

